Scientific Research Publishing

Open Journal of Civil Engineering, 2026, 16(2), 226-248
https://www.scirp.org/journal/ojce
ISSN Online: 2164-3172
ISSN Print: 2164-3164

Effect of Pipe Mass Vertical Distribution on Seismic Demands in Industrial Steel Pipe Racks

Thierno Mouhamadou Samassa Ly, Alassane Wade

Department of Civil and Environmental Engineering, Kookmin University, Seoul, South Korea
Email: thiernomsly100@gmail.com, a.wade028@gmail.com

How to cite this paper: Ly, T.M.S. and Wade, A. (2026) Effect of Pipe Mass Vertical Distribution on Seismic Demands in Industrial Steel Pipe Racks. *Open Journal of Civil Engineering*, **16**, 226-248.
https://doi.org/10.4236/ojce.2026.162011

Received: May 7, 2026
Accepted: May 30, 2026
Published: June 2, 2026

Abstract

Industrial pipe rack structures support piping systems carrying hazardous fluids at multiple elevations. In current seismic design practice, pipe mass is typically idealised as uniformly distributed across all levels, yet the actual distribution varies considerably depending on the operational configuration. The structural consequences of this idealisation on nonlinear seismic demands have not been systematically investigated. This study examines the effect of vertical pipe mass distribution on the nonlinear seismic response of a representative multi-level steel pipe rack structure. A finite element model is developed in SAP2000 with fiber-section hinges and link elements for bracing. Four pipe mass distribution cases—uniform, top-heavy, bottom-heavy, and mid-concentrated—are defined with constant total pipe mass. Nonlinear time-history analyses are performed under eleven spectrally matched ground motion pairs applied separately in the longitudinal and transverse directions, yielding eighty-eight analysis runs. The uniform distribution produces the highest seismic demands in both directions, with a maximum interstory drift ratio of 7.19% (longitudinal) and 3.10% (transverse). The non-uniform distributions reduce the maximum interstory drift ratio by 45% - 59%, peak roof displacement by 34% - 59%, and normalised base shear by 64% - 71% relative to the uniform baseline. The demand reductions are driven by a fundamental period shift exceeding a factor of 2.5, repositioning the structure across distinct spectral regions. When assessed against performance limit states, the uniform case exceeds collapse prevention in the braced direction, while non-uniform cases remain within life safety in the transverse direction. The uniform pipe mass assumption is shown to be inherently conservative; accounting for the actual distribution could shift the performance classification by one or more levels and enable more economical designs.

Keywords

Pipe Rack, Seismic Response, Nonlinear Time-History Analysis, Mass

Distribution, Vertical Irregularity

1. Introduction

Petrochemical complexes, refineries, and liquefied natural gas (LNG) facilities comprise a wide array of structural and non-structural components whose failure under seismic loading can result in the release of hazardous materials, prolonged production interruption, and a significant threat to human life and the environment [1] [2]. Among these components, pipe rack structures represent a critical element, as they extend over considerable lengths to connect process units and support piping systems carrying flammable or toxic fluids at multiple elevations [3]. The seismic hazard posed by pipe racks is compounded by the fact that they also support ancillary equipment such as cable trays, air coolers, and instrumentation, making their dynamic behaviour inherently complex [1] [3].

In current engineering practice, the seismic design of pipe rack structures is typically performed with the effect of the supported piping system represented by lumped masses assigned at beam-column joints, without explicit modelling of the piping stiffness or dynamic interaction [3] [4]. Structural engineers model only the rack, while piping stress engineers analyse the piping system independently using floor response spectra generated from the rack analysis [4] [5]. This decoupled approach is partly driven by time constraints in project delivery and partly by the absence of specific code provisions governing such interaction. The European code EN 13480-3 [6] for metallic industrial piping does not prescribe guidelines for dynamic coupling, and the American code ASCE 7-22 [7] addresses the weight ratio of non-structural components to the supporting structure primarily in the context of equipment-type non-building structures rather than pipe racks. Di Sarno and Karagiannakis (2020) [1] demonstrated that the selection of seismic design parameters, such as the behaviour factor and importance class, remains insufficiently defined for pipe rack structures in both European and American codes.

Research on the seismic behaviour of pipe rack structures has expanded in recent years, though the body of literature remains limited compared to that of conventional building structures. Paolacci *et al.* (2011) [4] investigated the seismic analysis and component design of refinery piping systems, highlighting the inadequacy of existing design rules and the significance of the dynamic filtering effect of the supporting rack. De Luca di Roseto *et al.* (2017) [2] applied a performance-based design framework to a modular steel pipe rack using nonlinear time-history analysis (NLTHA) in SAP2000 and demonstrated that performance-based approaches yield safer designs with fewer uncertainties than prescriptive methods. Di Sarno and Karagiannakis (2020) [5] assessed the seismic fragility of a reinforced concrete pipe rack-piping system considering soil-structure interaction through incremental dynamic analysis (IDA), concluding

that both the piping system and soil deformability are critical factors affecting fragility. In a subsequent study, Karagiannakis and Di Sarno (2021) [8] performed a performance-based assessment of a reinforced concrete pipe rack accounting for dynamic coupling with steel pipes, finding that code provisions may require cross-section increases to maintain piping in the elastic range. Puttatt (2020) [3] carried out a seismic fragility assessment of a representative steel pipe rack adapted from a petrochemical complex using IDA in both the transverse and longitudinal directions, providing fragility curves for different performance levels. Collectively, these studies have advanced the understanding of pipe rack seismic behaviour; however, they share a common characteristic: the pipe mass distribution across the rack elevations is treated as a fixed, given input, and its influence on the structural response is not isolated as a parametric variable.

The effect of vertical mass irregularity on seismic response has been extensively studied in the context of building structures. Al-Ali and Krawinkler (1998) [9] systematically investigated the effects of vertical irregularities—including mass, stiffness, and strength—on the seismic behaviour of building frames, demonstrating that non-uniform mass distributions can significantly alter interstory drift profiles and concentrate demands at specific stories. More recently, Nady *et al.* (2022) [10] introduced an index to quantify the extent and position of vertical irregularities, including mass, in reinforced concrete buildings and showed that the location of the irregularity along the building height governs the severity of its impact. These findings from building engineering establish that vertical mass distribution is a structurally meaningful parameter; however, no analogous investigation has been conducted for industrial pipe rack structures, where the pipe mass can constitute a substantial fraction of the total seismic weight and its vertical distribution varies across operational configurations.

This gap has direct practical implications. In industrial pipe racks, heavy process lines (large-diameter, liquid-filled) may be concentrated at specific elevations depending on the operational phase and routing constraints, while lighter utility lines occupy other levels. If certain pipe mass distributions—such as top-heavy or mid-concentrated patterns—produce significantly different demand distributions than the uniform assumption commonly adopted in design, current procedures may be unconservative for specific operational configurations. To date, no study has systematically varied the vertical pipe mass distribution while holding the total pipe mass constant, thereby isolating this variable and quantifying its effect on nonlinear seismic demands.

The present study addresses this gap by investigating the effect of vertical pipe mass distribution on the nonlinear seismic response of a representative multi-level steel pipe rack structure. Four mass distribution cases—uniform, top-heavy, bottom-heavy, and mid-concentrated—are defined with constant total pipe mass and applied to a reference model adapted from Puttatt (2020) [3]. Nonlinear time-history analyses are performed using eleven pairs of bidirec-

tional ground motions spectrally matched to the ASCE 7-22 [7] design spectrum, consistent with the minimum number of records required by ASCE 7-22 Section 16.2.2 to permit the use of mean response quantities. The engineering demand parameters examined include the interstory drift ratio profile, maximum interstory drift ratio, peak roof displacement, and normalised peak base shear. The results are compared against the uniform baseline to determine whether the standard design assumption of uniform pipe mass distribution is conservative, unconservative, or adequate across the range of realistic operational configurations.

2. Reference Pipe Rack Model

2.1. Structural Configuration

The reference pipe rack structure adopted in this study is reproduced from the steel pipe rack described by Puttatt (2020) [3], which was adapted from an actual petrochemical complex located in a region of moderate seismicity. The structure is a multi-level steel frame measuring 42.0 m in the longitudinal direction and 7.5 m in the transverse direction, with seven bays of 6.0 m each. The total height is 25.0 m, with piping supported at four elevations (EL 5.0, 10.0, 15.0, and 20.0 m) and a cable tray level at EL 25.0 m. The lateral force-resisting system consists of moment-resisting frames (MRF) in the transverse direction and diagonal bracing in the longitudinal direction. Secondary beams are provided between the main frames to support small-diameter pipes and are laterally restrained by struts and plan bracing. Large-diameter pipes are supported directly on the main frames. All column bases are modelled as pinned.

The structural members consist of European HE-series wide-flange sections of steel grade S275 (f_y = 275 MPa). The member sizes vary along the height of the structure, with heavier sections assigned to the lower levels where gravity and seismic demands are greatest. The member assignments are summarised in Table 1. A schematic of the structural configuration showing the three-dimensional view, the transverse elevation, and the longitudinal elevation is presented in Figure 1.

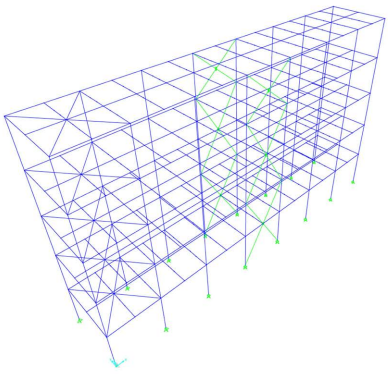

(a)

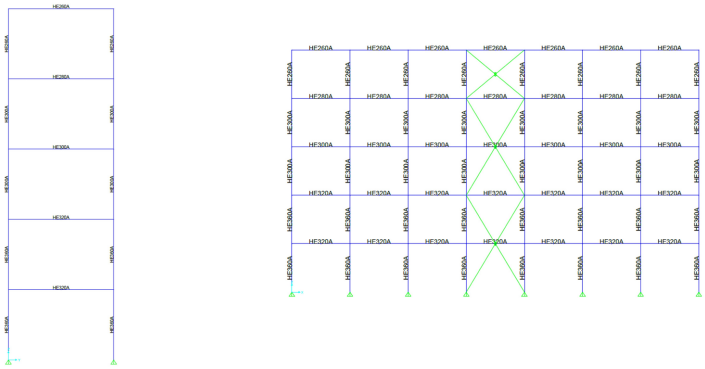

(b) (c)

Figure 1. Reference pipe rack structure: (a) three-dimensional view; (b) transverse elevation (MRF direction); (c) longitudinal elevation (braced direction). Adapted from Puttatt (2020) [3].

Table 1. Structural member assignments for the reference pipe rack model (after Puttatt (2020) [3]).

Element	Lower Levels	Upper Levels
Column (Transverse)	HE360A	HE300A
Columns (Longitudinal)	HE360A	HE300A
Main Beams (Transverse)	HE320A	HE260A
Main Beams (Longitudinal)	HE300A	HE260A
Secondary Beams	HE280A	HE260A
Diagonal Braces	Link Element	Link Element

2.2. Material Properties

All structural members are modelled using S275 European structural steel. A bi-linear stress-strain relationship with kinematic hardening is adopted, consistent with the material model used by Puttatt (2020) [3]. The key material parameters are: yield strength $f_y = 275$ MPa, elastic modulus $E = 210{,}000$ MPa, Poisson's ratio $\nu = 0.3$, strain-hardening ratio $b = 0.01$ (post-yield stiffness equal to 1% of the elastic stiffness), and steel density $\rho = 7{,}850$ kg/m^3. Geometric nonlinearity is accounted for through P-Δ effects in the analysis.

2.3. Nonlinear Modelling

The nonlinear finite element model is developed in SAP2000 [11]. Beam and column members are subdivided along their length into several sub-elements, with fiber-section hinges assigned at relative locations of 0.1 L and 0.9 L within each sub-element, where L denotes the sub-element length. This discretisation scheme approximates distributed plasticity by capturing the spread of yielding along the member length through multiple discrete fiber sections.

This approach is adopted to maintain consistency with the distributed inelas-

ticity modelling strategy employed by Puttatt (2020) [3], who used force-based (FB) distributed inelasticity elements with five integration points in SeismoStruct [12]. Although the software platforms differ, the underlying modelling philosophy is equivalent: both approaches capture nonlinear material behaviour at multiple sections along the member length through fiber discretisation, rather than relying on pre-defined lumped moment-rotation relationships.

For diagonal bracing members, the simulation of global buckling in compression is addressed through multi-linear link elements, following the approach of Puttatt (2020) [3]. The link elements are defined at coincident joints at the bracing ends and are characterised by an asymmetric bilinear force-displacement relationship that distinguishes between the tensile yield capacity and the reduced compressive buckling capacity of each brace. A link element with elastic stiffness of 17,298 kN/m, corresponding to an L50 × 50 × 5 angle section, is used. This formulation captures the essential hysteretic behaviour of bracing members under cyclic loading, including strength degradation following buckling.

2.4. Gravity Loads and Mass Assignment

The gravity loads are computed in accordance with the owner's engineering design specification as reported by Puttatt (2020) [3]. The dead load (DL) is taken as 1.20 kPa and the corresponding product load (PL) as 0.80 kPa, yielding a total operating load of 2.00 kPa at each pipe level. Since no live loads are anticipated during seismic events, the full values of gravity loads are considered for the computation of seismic masses. Masses are lumped at beam-column joints and divided equally among all joints at each elevation. The total pipe mass across the four pipe levels is 256.8 tonnes, with the cable tray level at EL 25.0 m carrying a fixed mass of 12.8 tonnes (see Section 3.1 for the distribution cases). The self-weight of the structural members is included automatically by the software. The distribution of dead and product loads per level is summarised in **Table 2**.

Table 2. Load distribution per level for pipe racks and cable trays.

Level	Beam Location	Trib. Width	DL (Dead)	PL (Live)
L1 - L4 (Pipe)	Interior (x = 6 to 36)	6.0 m	7.20 kN/m	4.80 kN/m
	Edge (x = 0 and 42)	3.0 m	3.60 kN/m	2.40 kN/m
L5 (Cable Tray)	Interior (x = 6 to 36)	6.0 m	2.40 kN/m	0
	Edge (x = 0 and 42)	3.0 m	1.20 kN/m	0

2.5. Baseline Model Verification

To verify that the SAP2000 baseline model reproduces the dynamic characteristics of the reference rack defined by Puttatt (2020) [3], an eigenvalue analysis was performed on each mass-distribution case and compared against the periods reported in the reference study. Puttatt reports first-mode periods of T_1 = 1.402 s in the transverse (MRF) direction and T_1 = 0.716 s in the longitudinal (braced) direction,

with cumulative mass-participation ratios exceeding 90% within the first three modes in both directions [3].

In the transverse direction, the four cases of the present model bracket Puttatt's reference value. The uniform case yields T_1, Y = 2.790 s, while the non-uniform cases yield T_1, Y = 1.041 - 1.200 s. The transverse direction is governed by the bending stiffness of the moment-resisting frames and is therefore sensitive to the total seismic mass and to its vertical distribution: the uniform case maximises the generalised mass associated with the first mode, lengthening the period, while the non-uniform cases relieve mass from the upper elevations and produce periods close to Puttatt's value. The bracketing of the reference period by the four cases is taken as evidence that the transverse-direction modelling—section properties, frame geometry, gravity-load to mass conversion, and connection assumptions—is consistent with the reference rack.

In the longitudinal direction, the present model produces first-mode periods longer than Puttatt's reported 0.716 s for all four cases. This discrepancy is attributable to the modelling of the diagonal bracing. Puttatt (2020) [3] illustrates the bracing idealisation through a generic asymmetric bilinear force-displacement schematic for the link element but does not specify the angle section adopted for the brace, the elastic stiffness of the link, the tensile yield force, or the post-buckling residual capacity. In the absence of these numerical specifications, the link element in the present study was independently defined with an elastic stiffness of 17,298 kN/m derived from the axial stiffness of an L50 × 50 × 5 angle, as reported in Section 2.3. This independently derived stiffness is evidently softer than the value implicitly used by Puttatt, lengthening the longitudinal-direction periods relative to the reference. Because Puttatt's link properties are not retrievable from the published material, exact agreement in the longitudinal direction is not achievable and is not pursued here.

Notwithstanding the longitudinal-direction period offset, the modal analysis of the present model reproduces the first-mode dominance reported by Puttatt, with more than 90% of the total mass captured within the first three modes in both directions, and the qualitative nonlinear response observed in Section 4—progressive brace buckling controlling the longitudinal direction and plastic-hinge formation controlling the transverse direction—is consistent with the mechanisms identified by Puttatt for the same reference rack. The baseline model is therefore considered to be dynamically consistent with the reference rack in those aspects that are fully specified in Puttatt (2020). The parametric comparisons in Section 4 are made between the four cases of the present model, not against the absolute response values of the reference, so the period offset in the longitudinal direction does not affect the conclusions of this study.

3. Parametric Study Design

3.1. Mass Distribution Cases

Four vertical pipe mass distribution cases are defined to investigate the sensitivity

of the seismic response to this parameter. In all cases, the total pipe mass is held constant at M_{total} = 256.8 tonnes, distributed across the four pipe levels (L1 = EL 5.0 m, L2 = EL 10.0 m, L3 = EL 15.0 m, L4 = EL 20.0 m). The cable tray mass at EL 25.0 m is fixed at 12.8 tonnes and is not redistributed. Lumped masses are assigned at beam-column joints, divided equally among all joints at each elevation. The four cases are defined in Table 3, and the corresponding per-joint mass values are reported in Table 4.

Case 1 (Uniform) represents the standard design assumption in which pipe mass is distributed equally across all pipe levels and serves as the baseline against which all other cases are compared. Case 2 (Top-Heavy) simulates a configuration in which heavy process lines are routed at the upper elevations, a scenario expected to amplify P-Δ effects and upper-story drift demands. Case 3 (Bottom-Heavy) represents the routing of heavy lines at lower levels, typically associated with grade-level equipment connections, which may increase base shear demands. Case 4 (Mid-Concentrated) models a major pipe corridor concentrated at mid-height, representative of a pipe bridge scenario, and tests the sensitivity of the response to mass concentration at a single elevation zone.

Table 3. Pipe mass distribution cases (percentage of M_total = 256.8 tonnes per level).

Level	Case 1	Case 2	Case 3	Case 4
L4 (EL 20 m)	25%	35%	18%	12%
L3 (EL 15 m)	25%	25%	22%	38%
L2 (EL 10 m)	25%	22%	25%	38%
L1 (EL 5 m)	25%	18%	35%	12%

Table 4. Pipe mass distribution per joint (16 joints per level).

Level	Case 1	Case 2	Case 3	Case 4
L4 (EL 20 m)	4.01 t	5.62 t	2.89 t	1.93 t
L3 (EL 15 m)	4.01 t	4.01 t	3.53 t	6.10 t
L2 (EL 10 m)	4.01 t	3.53 t	4.01 t	6.10 t
L1 (EL 5 m)	4.01 t	2.89 t	5.62 t	1.93 t
L5 (EL 25 m)	0.80 t	0.80 t	0.80 t	0.80 t
Total	269.6 t	269.6 t	269.6 t	269.6 t

3.2. Ground Motion Selection and Matching

Eleven pairs of bidirectional ground motion records are selected from the PEER NGA-West2 database [13]. The metadata of the selected records, station name, rupture distance Rrup, and shear-wave velocity Vs30 are reported in Table 5. The records were chosen according to the following criteria to ensure compatibility with the seismotectonic context and the characteristics of the reference structure. Records were restricted to shallow crustal earthquakes with moment magnitudes

M_w in the range 6.5 - 7.5 and rupture distances R_{rup} not exceeding 30 km, consistent with the dominant seismic hazard scenario for moderate-to-high seismicity regions in which petrochemical facilities are typically sited [14]. The magnitude range was selected to capture ground motions with sufficient energy content in the period range of interest ($0.2\,T_1$ to $2.0\,T_1$, spanning approximately 0.2 s to 5.6 s for the uniform case), while the distance constraint ensures that near-source directivity effects are not excluded [15].

The target design spectrum is constructed in accordance with ASCE 7-22 [7] for South Fork Long Canyon. The structure is assigned to Risk Category III, as pipe rack structures in petrochemical facilities support piping systems carrying hazardous materials whose failure could pose a substantial risk to human life and the environment, satisfying the criteria of ASCE 7-22. The site is classified as Site Class D (default soil type D recommended by ASCE), and the mapped spectral acceleration parameters are $S_S = 0.78$ g and $S_1 = 0.273$ g, consistent with the moderate seismic region described in Puttatt (2020) [3].

Table 5. Selected ground motion records.

No.	Earthquake	Year	Station	RSN	Vs30 (m/s)	Mw	Rrup (km)
1	Tabas	1978	Dayhook	139	471.53	7.35	13.94
2	Northridge	1994	Pacoima Kagel Canyon	1052	508.8	6.69	7.26
3	Kobe	1995	Kobe University	1108	1043.0	6.90	0.92
4	Superstition Hills	1987	Parachute Test Site	723	348.69	6.54	0.95
5	Superstition Hills	1987	Poe Road (Temp)	725	316.64	6.54	11.16
6	Erzincan	1992	Erzincan	821	352.05	6.69	4.38
7	Landers	1992	Joshua Tree	864	379.32	7.28	11.03
8	Manjil	1990	Abbar	1633	723.95	7.37	12.55
9	Cape Mendocino	1992	Cape Mendocino	825	567.78	7.01	6.96
10	Cape Mendocino	1992	Cape Mendocino	828	422.17	7.01	8.18
11	Corinth	1981	Corinth	313	361.4	6.60	10.27

Spectral matching was performed using SeismoMatch [16], which employs the wavelet-based algorithm proposed by Al Atik and Abrahamson (2010) [17]. This algorithm adjusts the frequency content of each record to match the target spectrum while preserving the non-stationary characteristics of the original ground motion, including the phasing, duration, and Arias intensity distribution. The matching was applied over the period range $0.2\,T_1$ to $2.0\,T_1$ of the uniform mass distribution case (Case 1), which encompasses the fundamental periods of all four cases. A matching tolerance of ±10% relative to the target spectral ordinate was enforced across the matching period range. Both horizontal components of each record were matched independently to the target spectrum, yielding 22 matched accelerograms (11 pairs). The quality of the spectral match is verified in **Figure 2**,

which shows that the mean spectrum of the matched records closely follows the target spectrum across the full period range.

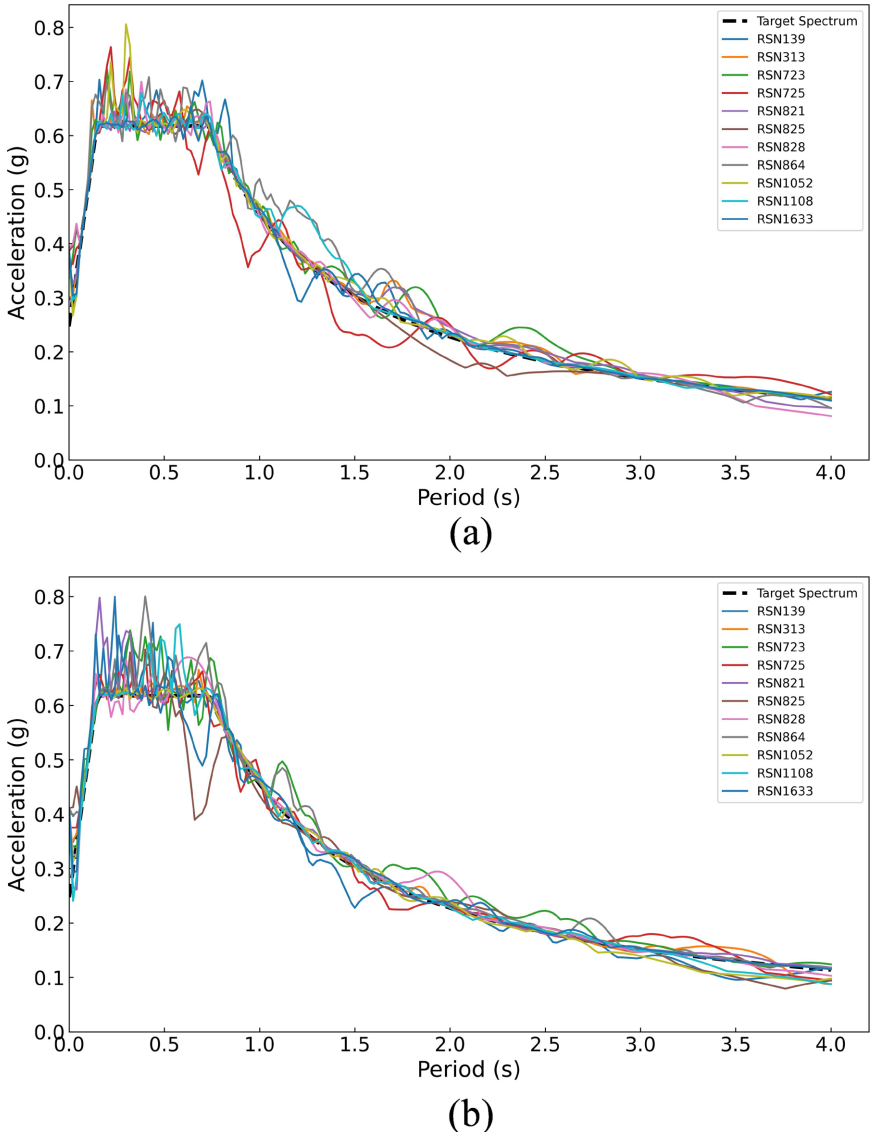

Figure 2. Response spectra of the eleven matched ground motion pairs compared with the ASCE 7-22 target design spectrum (5% damping): (a) X-direction; (b) Y-direction.

The use of spectral matching rather than amplitude scaling was adopted to minimise record-to-record variability in the spectral domain, thereby reducing the number of ground motions required for stable mean estimates [18] [19]. This approach is consistent with the recommendations of ASCE 41-17 [20] and has been shown to produce unbiased estimates of mean nonlinear structural response when applied over an appropriate period range [18]. The number of records is consistent with the minimum requirement of ASCE 7-22 [7] Section 16.2.2, which stipulates that when eleven or more ground motions are used in nonlinear response history analysis, the mean value of the response parameter of interest may

be used for design, rather than the more conservative maximum of the mean and the maximum response. The use of mean response is adopted in this study, as it provides a statistically stable estimate while maintaining computational tractability (4 cases × 11 pairs × 2 directions = 88 analysis runs).

3.3. Analysis Procedure

Nonlinear response history analyses are performed for all four mass distribution cases by applying each horizontal component of every ground-motion pair separately to the three-dimensional model. For each of the eleven pairs, the first horizontal component (H1) is applied along the longitudinal (X, braced) direction with no transverse excitation, and the second horizontal component (H2) is applied along the transverse (Y, MRF) direction with no longitudinal excitation. This yields 4 cases × 11 record pairs × 2 loading directions = 88 nonlinear time-history runs in total. The unidirectional excitation protocol was adopted to isolate the effect of pipe mass vertical distribution on the response in each principal direction without compounding contributions from cross-axis coupling, and is consistent with the parametric scope of the study. Simultaneous bidirectional excitation, while permitted by ASCE 7-22 [7] Section 16.2.4 for design verification of three-dimensional models, is not required for the comparative parametric assessment performed here and is identified as a topic for future work in Section 5.

Viscous damping is modelled using Rayleigh damping (mass- and stiffness-proportional) with a damping ratio of 5% of critical, specified at two control periods: T_1, taken equal to the fundamental period of the case under analysis, and T_2, taken equal to the period of the higher mode at which the cumulative mass-participation ratio first exceeds 90% for that case. Anchoring T_1 at the fundamental period suppresses spurious damping of the first mode, while anchoring T_2 at the 90%-MPR mode prevents over-damping of the higher modes that contribute to the seismic response. The mass-proportional coefficient α and stiffness-proportional coefficient β are computed automatically by SAP2000 from these two control periods at 5% critical damping, in accordance with Equation (1) and Equation (2), where $\xi = 0.05$, $\omega_1 = 2\pi/T_1$, and $\omega_2 = 2\pi/T_2$.

The stiffness-proportional component of Rayleigh damping is formulated on the initial elastic stiffness matrix, consistent with the SAP2000 default for Direct Integration nonlinear time-history load cases. No supplementary control was applied to suppress artificial damping after yielding or brace buckling; the Rayleigh formulation defined above was the only viscous-damping source throughout the analysis. The 5% damping ratio is consistent with the conventional assumption for steel structures and with the damping level implicit in the ASCE 7-22 design spectrum [7]. Time integration was performed using the HHT-α method as implemented in SAP2000, which provides controlled high-frequency numerical dissipation without affecting the response in the period range of interest.

$$\alpha = 2\xi\omega_1\omega_2 / (\omega_1 + \omega_2) \tag{1}$$

$$\beta = 2\xi / (\omega_1 + \omega_2) \tag{2}$$

The analysis procedure is automated using the SAP2000 Open Application Programming Interface (OAPI) through Python scripting, which enables batch execution of all 88 runs and systematic extraction of the following engineering demand parameters (EDPs) from each analysis: i) peak interstory drift ratio (IDR) at each level; ii) maximum interstory drift ratio (MIDR), defined as the maximum of the IDR profile; iii) peak roof displacement; and iv) peak base shear, normalised by the seismic weight (V/W). For each mass distribution case, the mean value of each EDP across the eleven ground motions is computed for each loading direction and used as the representative response quantity.

4. Results and Discussion

4.1. Modal Analysis Results

The modal properties obtained from eigenvalue analysis for each mass distribution case are summarised in Table 6. For each case, the table reports the fundamental period and mass participation ratio (MPR) corresponding to the dominant translational mode in the longitudinal (X, braced) and transverse (Y, MRF) directions, together with the first three modal periods.

Table 6. Fundamental modal properties for each mass distribution case.

Parameter	Case 1 Uniform	Case 2 Top-Heavy	Case 3 Bottom-Heavy	Case 4 Mid-Conc.
Longitudinal Direction (X, Braced)				
T1, X (s)	2.593	1.057	0.951	1.043
MPR (X)	0.928	0.935	0.922	0.915
Transverse Direction (Y, MRF)				
T1, Y (s)	2.790	1.200	1.041	1.062
MPR (Y)	0.800	0.813	0.785	0.791
First Three Modal Periods (s)				
Mode 1	2.790	1.200	1.041	1.062
Mode 2	2.692	1.130	0.974	1.043
Mode 3	2.593	1.057	0.951	1.000

The results reveal a substantial influence of the pipe mass distribution on the dynamic characteristics of the structure. The uniform distribution (Case 1) yields the longest fundamental periods in both directions (T1, Y = 2.790 s, T1, X = 2.593 s), while the non-uniform distributions produce significantly shorter periods, ranging from 0.951 s to 1.200 s. This difference is attributable to the manner in which the equal distribution of mass across all pipe levels in Case 1 results in a higher effective mass at upper elevations relative to the non-uniform cases, thereby increasing the generalised mass associated with the first mode and elongating the period. In contrast, the non-uniform cases concentrate mass at specific levels, shifting the effective modal height and reducing the contribution of upper-level mass to the first mode.

The mass participation ratios are relatively consistent across all cases, with the first mode capturing approximately 79% - 81% of the total mass in the transverse direction and 92% - 94% in the longitudinal direction. The structural response is therefore governed by the first mode in both directions, with more than 90% of the total mass captured within the first three modes, consistent with the findings of Puttatt (2020) [3] for the reference configuration. This first-mode dominance is a characteristic feature of pipe rack structures due to the absence of floor diaphragms and the relatively uniform stiffness distribution along the height [1].

4.2. Interstory Drift Response

The mean interstory drift ratio (IDR) height profiles for all four mass distribution cases are presented in Figure 3, with subplots showing the longitudinal (X) and transverse (Y) directions separately. The corresponding maximum interstory drift ratio (MIDR) values are compared in Figure 4 and summarised in Table 7.

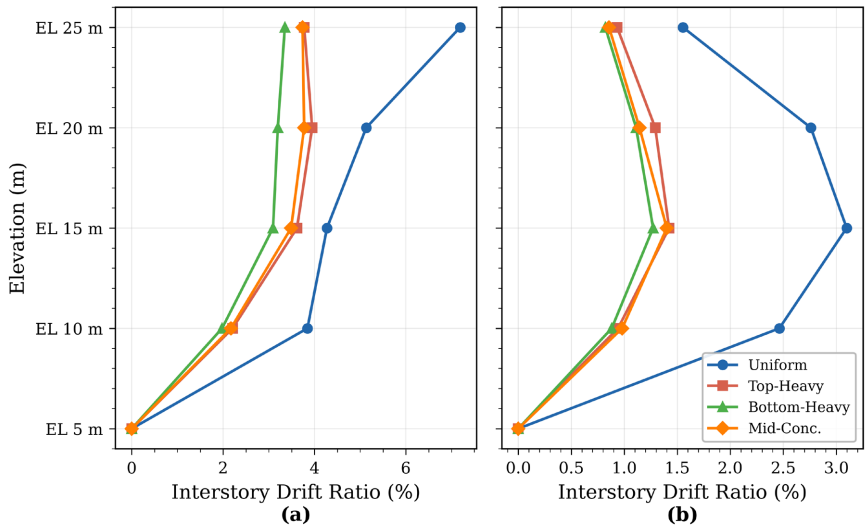

Figure 3. Mean interstory drift ratio height profiles: (a) longitudinal direction (X); (b) transverse direction (Y).

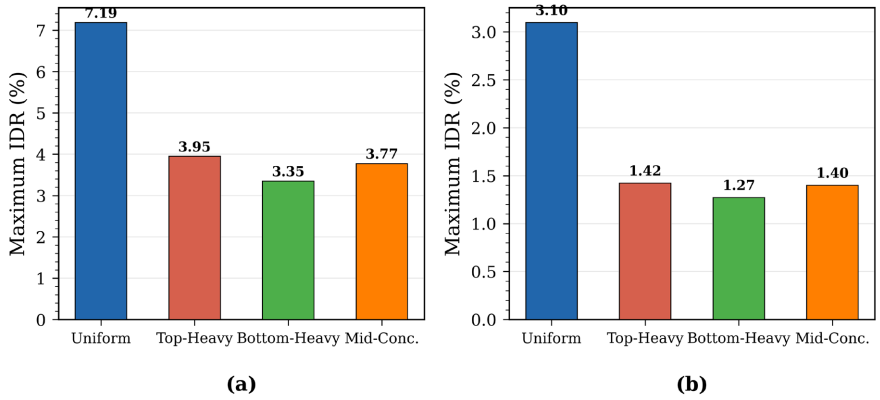

Figure 4. Mean maximum interstory drift ratio (MIDR): (a) longitudinal direction (X); (b) transverse direction (Y).

Table 7. Summary of mean peak response quantities for each mass distribution case.

Case	Longitudinal (X)			Transverse (Y)		
	MIDR (%)	Roof (mm)	V/W (%)	MIDR (%)	Roof (mm)	V/W (%)
1 (Uniform)	7.19	1022.1	16.49	3.10	493.7	39.01
2 (Top-Heavy)	3.95	677.4	5.25	1.42	231.7	13.48
3 (Bottom-Heavy)	3.35	580.9	4.84	1.27	205.0	12.80
4 (Mid-Conc.)	3.77	658.5	5.22	1.40	219.7	14.15

In the longitudinal direction (Figure 3(a)), the uniform distribution (Case 1) exhibits the highest IDR values at all elevations, with the peak drift occurring at the top level (EL 25 m), reaching 7.19%. This pronounced concentration of drift at the upper story is consistent with the softening behaviour expected from progressive brace buckling under strong ground shaking, as observed by Puttatt (2020) [3] in the same reference structure. The non-uniform cases (Cases 2 - 4) produce substantially lower IDR profiles, with MIDR values ranging from 3.35% (Case 3, Bottom-Heavy) to 3.95% (Case 2, Top-Heavy), representing reductions of 45.1% to 53.4% relative to the uniform baseline.

In the transverse direction (Figure 3(b)), a similar trend is observed, though at lower absolute magnitudes owing to the greater flexibility and energy dissipation capacity of the moment-resisting frames. The uniform case produces an MIDR of 3.10% at EL 15 m, while the non-uniform cases yield MIDR values between 1.27% and 1.42%, corresponding to reductions of 54.1% to 58.9%. The drift profiles for the non-uniform cases are notably more compact and shifted toward the lower elevations compared to the uniform case.

The observation that the uniform distribution consistently produces the highest drift demands in both directions is a counterintuitive but physically explicable result. The substantially longer fundamental period of the uniform case (Table 6) positions the structure in a more displacement-sensitive region of the response spectrum, resulting in larger spectral displacement demands. Furthermore, the uniform distribution of mass across all levels maximises the effective modal height, thereby amplifying the displacement response at upper elevations. This finding has direct design implications, as discussed in Section 4.5.

4.3. Peak Roof Displacement and Base Shear

The peak roof displacement and normalised base shear (V/W) for each mass distribution case are shown in Figure 5 and Figure 6, respectively, and are summarised alongside the MIDR values in Table 7. The percentage changes relative to the uniform baseline are presented in Table 8.

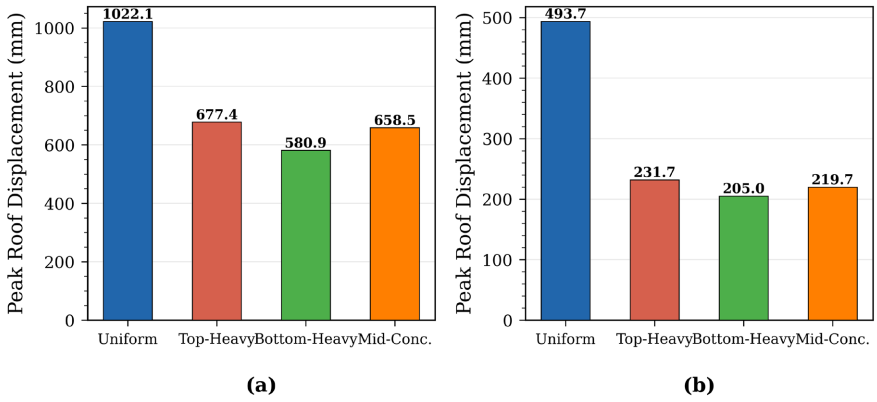

Figure 5. Mean peak roof displacement: (a) longitudinal direction (X); (b) transverse direction (Y).

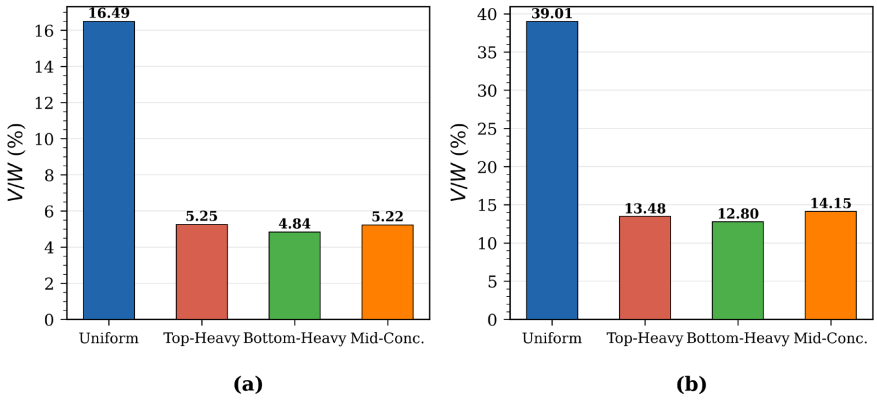

Figure 6. Mean normalised peak base shear (V/W): (a) longitudinal direction (X); (b) transverse direction (Y).

Table 8. Percentage change in mean peak response quantities relative to the uniform baseline (Case 1).

Case	Longitudinal (X)			Transverse (Y)		
	ΔMIDR	ΔRoof	ΔV/W	ΔMIDR	ΔRoof	ΔV/W
2 (Top-Heavy)	−45.1%	−33.7%	−68.2%	−54.1%	−53.1%	−65.4%
3 (Bottom-Heavy)	−53.4%	−43.2%	−70.7%	−58.9%	−58.5%	−67.2%
4 (Mid-Conc.)	−47.5%	−35.6%	−68.3%	−54.8%	−55.5%	−63.7%

To verify that the ranking of the four mass-distribution cases is stable across the eleven records and is not an artefact of the mean operation, the record-to-record dispersion of each engineering demand parameter was computed. Standard deviation (SD) and coefficient of variation (CoV) across the eleven pairs are reported in Table 9 together with the minimum and maximum response over the suite. The CoV ranges from 6% to 18% in the transverse direction and from 6% to 33% in the longitudinal direction, the higher dispersion in the longitudinal direction reflecting the well-known sensitivity of braced-frame response to the post-

buckling sequence under individual records. The mean ranking—Case 1 producing the largest demands and Case 3 producing the smallest—is preserved record-by-record in the transverse direction for all eleven pairs, and in nine of the eleven pairs in the longitudinal direction. The dispersion, therefore, confirms that the demand reductions reported in Table 8 are stable and not driven by outlier records.

Table 9. Record-to-record dispersion of engineering demand parameters across the eleven ground-motion pairs (n = 11).

Case	DIR.	EDP	Mean	SD	COV	Min	Max
1	X	MIDR (%)	7.31	1.25	17.1	5.16	9.02
		Roof (mm)	1022.1	132.7	13.0	733.5	1133.7
		V/W (%)	16.49	2.81	17.1	12.28	22.00
	Y	MIDR(%)	3.17	0.52	16.4	2.42	4.08
		Roof (mm)	493.7	69.4	14.1	413.3	611.8
		V/W (%)	39.01	3.51	9.0	33.40	43.55
2	X	MIDR (%)	4.18	0.73	17.5	3.29	5.29
		Roof (mm)	677.4	108.0	15.9	549.3	863.7
		V/W (%)	5.25	1.55	29.4	4.29	9.60
	Y	MIDR (%)	1.42	0.10	6.9	1.29	1.53
		Roof (mm)	231.7	18.0	7.8	202.9	263.1
		V/W (%)	13.48	0.85	6.3	12.12	14.63
3	X	MIDR (%)	3.59	1.19	33.2	2.03	5.72
		Roof (mm)	580.9	152.8	26.3	351.6	821.6
		V/W (%)	4.84	0.79	16.2	4.29	6.91
	Y	MIDR (%)	1.30	0.12	9.0	1.07	1.46
		Roof (mm)	205.0	21.1	10.3	160.7	237.3
		V/W (%)	12.80	0.85	6.6	11.85	14.56
4	X	MIDR (%)	4.14	1.20	29.0	2.99	6.45
		Roof (mm)	658.5	155.7	23.6	468.4	924.9
		V/W (%)	5.22	1.48	28.4	3.97	8.89
	Y	MIDR (%)	1.41	0.13	9.6	1.07	1.54
		Roof (mm)	219.7	20.1	9.1	175.8	242.7
		V/W (%)	14.15	1.06	7.5	12.39	15.64

The peak roof displacement follows the same trend as the MIDR. In the longitudinal direction, the uniform case produces a mean roof displacement of 1022.1 mm, which reduces to 580.9 - 677.4 mm for the non-uniform cases (reductions of 33.7% to 43.2%). In the transverse direction, the corresponding reduction is from

493.7 mm to 205.0 - 231.7 mm (reductions of 53.1% to 58.5%). The bottom-heavy distribution (Case 3) consistently yields the lowest displacement demands in both directions, attributable to the concentration of mass at lower elevations, which reduces the effective modal height and, consequently, the displacement amplification along the height of the structure [9].

The normalised base shear (V/W) exhibits a pronounced sensitivity to the mass distribution. The uniform case produces V/W values of 16.49% and 39.01% in the longitudinal and transverse directions, respectively, while the non-uniform cases yield values ranging from 4.84% to 5.25% (X) and 12.80% to 14.15% (Y), representing reductions of 68% - 71% (X) and 64% - 67% (Y) relative to the uniform baseline. To distinguish the contribution of elastic spectral effects from that of nonlinear yielding and buckling, the 5%-damped ASCE 7-22 design-spectrum ordinates at T_1 are reported for each case in **Table 10**.

Table 10. ASCE 7-22 design-spectrum ordinates Sa (T_1, 5%) at the fundamental period of each case.

Case	T1, X (s)	Sa (T1, X) (s)	T1, Y (s)	Sa (T1, Y) (s)	Sa Case 1/Sa Case j (x)	Sa Case 1/Sa Case j (Y)
1	2.593	0.114	2.790	0.106	—	—
2	1.057	0.280	1.200	0.247	0.41	0.43
3	0.951	0.311	1.041	0.284	0.37	0.37
4	1.043	0.284	1.062	0.279	0.40	0.38

Table 11 reveals that the uniform case sits on the descending velocity-sensitive branch of the spectrum ($T_1 \approx 2.6$ - 2.8 s, Sa ≈ 0.11g), while the non-uniform cases sit near the plateau ($T_1 \approx 1.0$ - 1.2 s, Sa ≈ 0.25 g - 0.31 g). The elastic spectral demand at the fundamental period is therefore 2.4 - 2.7 times larger for the non-uniform cases than for the uniform case—that is, the period shift on its own would predict an increase in base shear for Cases 2 - 4 relative to Case 1, not the observed reduction of 64% - 71%.

Table 11. Comparison of mean MIDR values against FEMA 356 indicative performance drift limits.

Case	MIDR (X) (%)	MIDR (Y) (%)	Indicative Performance Level
1 (Uniform)	7.19	3.10	>CP (long.); LS-CP (trans.)
2 (Top-Heavy)	3.95	1.42	>CP (long.); IO-LS (trans.)
3 (Bottom-Heavy)	3.35	1.27	>CP (long.); IO-LS (trans.)
4 (Mid-Conc.)	3.77	1.40	>CP (long.); IO-LS (trans.)

FEMA 356 indicative drift limits for reference: Braced frame (long.): IO ≈ 0.5%, LS ≈ 1.5%, CP ≈ 2.0%; MRF (trans.): IO ≈ 0.7%, LS ≈ 2.0%, CP ≈ 5.0%.

The observed reduction must therefore be attributed predominantly to nonlin-

ear effects. The uniform case enters a strongly nonlinear regime under all eleven records: extensive brace buckling in the longitudinal direction and significant plastic-hinge formation in the transverse direction MRF beams. The base shear of Case 1 reflects the post-buckling residual capacity of the structure (*i.e.*, a capacity-limited response), and the very large MIDR of 7.19% (longitudinal) is a direct consequence of this softening combined with the long fundamental period that places the structure in a displacement-sensitive region. In contrast, the non-uniform cases experience comparatively limited yielding and only localised buckling, so their base shear approaches the elastic-spectrum demand reduced by moderate ductility. The 64% - 71% reduction in V/W is therefore best understood as the combined outcome of i) a long-period uniform-case response that is capacity-limited by widespread brace buckling and plastic hinging, and ii) shorter-period non-uniform cases that respond near the elastic plateau without comparable softening. Period-dependent elastic spectral effects [7], [21] are present but, on their own, would act in the opposite direction; the dominant mechanism is the difference in nonlinear inelastic engagement between the cases.

Among the non-uniform distributions, the mid-concentrated case (Case 4) produces slightly higher base shear in the transverse direction (V/W = 14.15%) compared to Cases 2 and 3. This is consistent with the observation that concentrating mass at mid-height elevations generates a higher effective seismic force for the MRF system, where the mode shape amplitude is maximum near mid-height [21].

4.4. Assessment against Performance Limit States

To contextualise the computed drift demands within a performance-based framework, the mean MIDR values obtained for each mass distribution case are compared against the interstory drift acceptance criteria prescribed by ASCE 41-17 [20] and FEMA 356 [22] for steel structures. Although these standards were developed primarily for building structures, they are commonly applied to building-like non-building structures such as pipe racks in the absence of dedicated performance criteria [1] [3]. The applicable drift limits depend on the structural system type and the target performance level: Immediate Occupancy (IO), Life Safety (LS), and Collapse Prevention (CP). To place the computed drift demands in context, the mean MIDR values obtained for each mass distribution case are compared with the indicative interstory drift thresholds reported in FEMA 356 [22] for steel structures. The FEMA 356 thresholds were developed for steel buildings; they are not formal acceptance criteria for industrial pipe racks, and the present comparison is therefore made strictly for comparative purposes between the four mass-distribution cases rather than as a performance verification of the rack. The comparison highlights the relative shift in performance classification that the assumed pipe mass distribution can induce; it does not constitute a substitute for a component-level performance assessment.

For steel moment-resisting frames (transverse direction), FEMA 356 [22] Table C1-3 reports indicative interstory drift values of approximately 0.7% (IO), 2.5%

(LS), and 5.0% (CP). For steel concentrically braced frames (longitudinal direction), the corresponding indicative values are approximately 0.5%, 1.5%, and 2.0%. ASCE 41-17 [20], which superseded FEMA 356, prescribes acceptance criteria at the component level (plastic rotation of beams and columns, axial deformation of bracing members, and so on) rather than global interstory-drift limits. A formal performance-based assessment of the rack in accordance with ASCE 41-17 would require these component-level checks to be evaluated for the most-stressed members under each case; such checks were not performed in the present parametric study and are identified as future work. The FEMA 356 global drift thresholds are therefore retained here only as approximate global indicators against which the relative performance of the four mass-distribution cases can be compared.

Table 11 summarises the assessment. In the longitudinal direction, the uniform case (Case 1) produces an MIDR of 7.19%, which substantially exceeds the CP threshold of 2.0% for braced frames, indicating that the structure under this mass configuration would be classified as experiencing collapse-level demands. The non-uniform cases yield MIDR values of 3.35% - 3.95%, which also exceed the CP limit but by a considerably smaller margin. In the transverse direction, the uniform case produces an MIDR of 3.10%, which exceeds the LS limit of 2.0% but remains below the CP threshold of 5.0%, placing it in the LS-CP range. The non-uniform cases yield MIDR values of 1.27% - 1.42%, placing them within the IO-LS range—a markedly more favourable performance classification.

These results underscore two important points. First, the longitudinal (braced) direction is the critical direction for all mass distribution cases, with all cases exceeding the CP drift limit. This is consistent with the progressive brace buckling mechanism observed in the IDR profiles (**Figure 3(a)**) and with the findings of Puttatt (2020) [3], who similarly reported that the CP limit state could not be verified in the braced direction. Second, the difference in performance classification between the uniform and non-uniform cases is pronounced in the transverse direction: the uniform case falls in the LS-CP range, while the non-uniform cases remain within the IO-LS range. This demonstrates that the assumed pipe mass distribution can shift the performance assessment outcome by one or more performance levels, reinforcing the practical significance of the parametric variable investigated in this study. It is reiterated that the performance classifications presented in **Table 9** are indicative only, derived from global drift thresholds developed for steel buildings and applied here for comparative purposes between cases. A formal performance-based assessment of the rack would require component-level acceptance checks per ASCE 41-17 [20] (plastic rotations of beam and column elements, axial deformation demands on the bracing link elements, and member-by-member chord rotations), which were not performed in this parametric study and are identified as a topic for future work.

4.5. Design Implications

The results of this parametric study yield several findings with direct relevance to

the seismic design practice of industrial pipe rack structures.

First, the uniform mass distribution assumption, commonly adopted in design practice for simplicity, is shown to be the most conservative case across all engineering demand parameters and both structural directions. The non-uniform distributions consistently produce lower MIDR, roof displacement, and base shear demands by margins ranging from 34% to 71%. This finding suggests that the uniform assumption provides an inherent safety margin that is not explicitly recognised in current design codes [7] [1]. From a design verification perspective, this is a favourable outcome: engineers who design pipe racks under the uniform mass assumption are unlikely to underestimate the seismic demands for any realistic operational configuration.

Second, the sensitivity of the structural response to the mass distribution is primarily mediated through the fundamental period. The uniform distribution, by spreading mass equally across all levels, maximises the generalised mass associated with the first mode and elongates the fundamental period, placing the structure in a more displacement- and acceleration-sensitive region of the response spectrum. This mechanism is analogous to the effect of vertical mass irregularity in building structures, where floors with concentrated mass attract higher seismic demands [9] [10]. However, the effect observed here operates in the opposite direction: the uniform distribution, by virtue of its higher effective modal mass, produces the most severe response.

Third, the bottom-heavy distribution (Case 3) yields the lowest demands across nearly all EDPs, suggesting that configurations in which heavy process lines are routed at lower elevations are inherently beneficial from a seismic perspective. This finding is consistent with the general principle that lowering the centre of mass reduces overturning demands and the effective modal height [21].

Fourth, the magnitude of variation observed—up to 71% reduction in base shear and 59% reduction in MIDR—is sufficiently large to warrant consideration in design optimisation. While the uniform assumption remains conservative, the substantial over-prediction of demands may lead to unnecessarily heavy member sections, particularly in the longitudinal (braced) direction where the baseline MIDR exceeds 7%. This over-design could be mitigated by accounting for the actual pipe mass distribution when it is known at the detailed engineering stage, as recommended by Di Sarno and Karagiannakis (2020) [1] for the general case of pipe rack design.

It should be noted that the present study considers the pipe mass as lumped at beam-column joints without modelling the dynamic interaction between the piping system and the supporting structure. As demonstrated by Di Sarno and Karagiannakis (2020) [5] and Karagiannakis and Di Sarno (2021) [8], the coupling between the piping system and the rack can modify the seismic demands, particularly at elevations where heavy pipes are concentrated. The trends identified in this study may therefore be modulated when pipe-structure interaction is explicitly considered, and this aspect is recommended for future investigation.

5. Conclusions

This study investigated the effect of vertical pipe mass distribution on the nonlinear seismic response of a representative multi-level steel pipe rack structure through nonlinear time-history analysis. Four mass distribution cases—uniform, top-heavy, bottom-heavy, and mid-concentrated—were analysed under eleven spectrally matched ground motion pairs applied separately in the longitudinal and transverse directions (88 analysis runs). The principal findings are as follows.

1) The vertical distribution of pipe mass has a substantial influence on the dynamic characteristics and nonlinear seismic demands of the pipe rack structure. The fundamental period varied by a factor of approximately 2.5 between the uniform and non-uniform cases (2.79 s versus 1.04 - 1.20 s in the transverse direction), despite the total seismic mass remaining constant.

2) The uniform mass distribution consistently produced the highest seismic demands across all engineering demand parameters (MIDR, peak roof displacement, and normalised base shear) and in both structural directions. This finding indicates that the common design practice of assuming uniform pipe mass distribution is inherently conservative and does not underestimate seismic demands for any of the non-uniform configurations considered.

3) The magnitude of the demand reduction for non-uniform distributions relative to the uniform baseline is significant: 45% - 59% for MIDR, 34% - 59% for peak roof displacement, and 64% - 71% for normalised base shear (V/W). These reductions are primarily attributable to the shortening of the fundamental period, which shifts the structural response to a less demanding region of the design spectrum.

4) Among the non-uniform distributions, the bottom-heavy configuration (Case 3) produced the lowest demands across nearly all EDPs, while the top-heavy configuration (Case 2) produced the highest demands among the non-uniform cases. The mid-concentrated case (Case 4) yielded intermediate results.

5) When assessed against the indicative drift limits of FEMA 356 [22], the pipe mass distribution was found to affect the performance classification. In the transverse (MRF) direction, the uniform case falls within the Life Safety-Collapse Prevention range (MIDR = 3.10%), whereas the non-uniform cases remain within the Immediate Occupancy-Life Safety range (MIDR = 1.27% - 1.42%). In the longitudinal (braced) direction, all cases exceed the Collapse Prevention limit, consistent with progressive brace buckling.

6) The longitudinal (braced) direction exhibited higher drift demands than the transverse (MRF) direction for the uniform case (MIDR of 7.19% versus 3.10%), consistent with the progressive brace buckling mechanism. This directional sensitivity was less pronounced for the non-uniform cases.

7) While the conservatism of the uniform assumption is beneficial for design safety, the substantial over-prediction of demands (up to 71% in base shear) may result in unnecessarily conservative member sizing. When the actual pipe mass distribution is known at the detailed engineering stage, accounting for its effect

on seismic demands could enable more economical designs without compromising safety.

Future research should extend this investigation to consider i) the dynamic interaction between the piping system and the supporting structure, ii) the effect of horizontal mass distribution and plan eccentricity, iii) bidirectional simultaneous excitation, and iv) incremental dynamic analysis to quantify the sensitivity across a range of seismic intensity levels rather than at a single design-level hazard.

Conflicts of Interest

The authors declare no conflicts of interest regarding the publication of this paper.

References

[1] Di Sarno, L. and Karagiannakis, G. (2020) Petrochemical Steel Pipe Rack: Critical Assessment of Existing Design Code Provisions and a Case Study. *International Journal of Steel Structures*, **20**, 232-246. https://doi.org/10.1007/s13296-019-00280-w

[2] di Roseto, A.d.L., Palmeri, A. and Gibb, A.G. (2017) Performance-Based Seismic Design of a Modular Pipe-Rack. *Procedia Engineering*, **199**, 3564-3569. https://doi.org/10.1016/j.proeng.2017.09.519

[3] Jayarajan, P. (2020) Seismic Fragility Assessment of a Pipe Rack Structure in a Petrochemical Complex by Incremental Dynamic Analysis. *Journal of Structural Engineering* (*Madras*), **47**, 408-415. https://www.academia.edu/44791802/Seismic_fragility_assessment_of_a_pipe_rack_structure_in_a_petrochemical_complex_by_incremental_dynamic_analysis

[4] Paolacci, F., Reza, M.S. and Bursi, O.S. (2011) Seismic Analysis and Component Design of Refinery Piping Systems. *III ECCOMAS Thematic Conference on Computational Methods in Structural Dynamics and Earthquake Engineering* (*COMPDYN* 2011), Corfu, 25-28 May 2011, 1-24. https://congress.cimne.com/eccomas/proceedings/compdyn2011/compdyn2011_full/360.pdf

[5] Di Sarno, L. and Karagiannakis, G. (2020) On the Seismic Fragility of Pipe Rack—Piping Systems Considering Soil-Structure Interaction. *Bulletin of Earthquake Engineering*, **18**, 2723-2757. https://doi.org/10.1007/s10518-020-00797-0

[6] European Committee for Standardization (CEN) (2012) Metallic Industrial Piping-Part 3: Design and Calculation. EN 13480-3:2012.

[7] ASCE/SEI (2022) Minimum Design Loads and Associated Criteria for Buildings and Other Structures. ASCE/SEI 7-22, American Society of Civil Engineers.

[8] Karagiannakis, G. and Di Sarno, L. (2021) Seismic Performance-Based Assessment of a RC Pipe Rack Accounting for Dynamic Interaction. *Structures*, **34**, 1338-1352.

[9] Al-Ali, A.A.K. and Krawinkler, H. (1998) Effects of Vertical Irregularities on Seismic Behavior of Building Structures. Report No. 130, John A. Blume Earthquake Engineering Center, Stanford University. https://purl.stanford.edu/qh189ph3062

[10] Nady, O., Mahfouz, S.Y. and Taher, S.E.F. (2022) Quantification of Vertical Irregularities for Earthquake Resistant Reinforced Concrete Buildings. *Buildings*, **12**, Article No. 1160. https://doi.org/10.3390/buildings12081160

[11] Computers and Structures, Inc. (2025) SAP2000: Linear and Nonlinear Static and Dynamic Analysis of Three-Dimensional Structures. CSI.

[12] Seismosoft (2018) SeismoStruct—The Ultimate Finite Element Package for Seismic Analysis. https://seismosoft.com/products/seismostruct/

[13] Pacific Earthquake Engineering Research Center (PEER) (2013) PEER NGA-West2 Ground Motion Database. University of California. https://ngawest2.berkeley.edu

[14] Baker, J.W. (2011) Conditional Mean Spectrum: Tool for Ground-Motion Selection. *Journal of Structural Engineering*, **137**, 322-331. https://doi.org/10.1061/(asce)st.1943-541x.0000215

[15] Shahi, S.K. and Baker, J.W. (2014) An Efficient Algorithm to Identify Strong-Velocity Pulses in Multicomponent Ground Motions. *Bulletin of the Seismological Society of America*, **104**, 2456-2466. https://doi.org/10.1785/0120130191

[16] Seismosoft (2024) SeismoMatch—Precision Response Spectrum Matching. https://seismosoft.com/products/seismomatch/

[17] Al Atik, L. and Abrahamson, N. (2010) An Improved Method for Nonstationary Spectral Matching. *Earthquake Spectra*, **26**, 601-617. https://doi.org/10.1193/1.3459159

[18] Grant, D.N. and Diaferia, R. (2011) Assessing Adequacy of Spectrum-Matched Ground Motions for Nonlinear Dynamic Analysis. *Earthquake Engineering and Structural Dynamics*, **40**, 1293-1311.

[19] Heo, Y., Kunnath, S.K. and Abrahamson, N. (2011) Amplitude-Scaled versus Spectrum-Matched Ground Motions for Seismic Performance Assessment. *Journal of Structural Engineering*, **137**, 278-288. https://doi.org/10.1061/(asce)st.1943-541x.0000340

[20] ASCE/SEI (2017) Seismic Evaluation and Retrofit of Existing Buildings. ASCE/SEI 41-17, American Society of Civil Engineers.

[21] Chopra, A.K. (2020) Dynamics of Structures: Theory and Applications to Earthquake Engineering. 5th Edition, Pearson.

[22] Federal Emergency Management Agency (FEMA) (2000) Prestandard and Commentary for the Seismic Rehabilitation of Buildings. FEMA 356, Washington.